catalysts

MDPI

Article

Stability and Activity of Zn/MCM-41 Materials in Toluene Alkylation: Microwave Irradiation vs Continuous Flow

Paola M. Carraro [1], Bruna S. Goldani [2], Diego Alves [2], A. Gabriel Sathicq [3], Griselda A. Eimer [1], Gustavo P. Romanelli [3,4] and Rafael Luque [5,6,*]

1 Centro de Investigación y Tecnología Química (CITeQ), Universidad Tecnologica Nacional, Córdoba 5016, Argentina; paocarraro@gmail.com (P.M.C.); geimer@frc.utn.edu.ar (G.A.E.)
2 LASOL, CCQFA, Universidade Federal de Pelotas, UFPel, Pelotas 96010-610, Brazil; goldanibruna@gmail.com (B.S.G.); diego.alves@ufpel.edu.br (D.A.)
3 Centro de Investigación y Desarrollo en Ciencias Aplicadas "Dr. Jorge J. Ronco" (CINDECA-CCT La Plata-CONICET-CIC), Universidad Nacional de La Plata, La Plata B1900AJK, Argentina; agsathicq@quimica.unlp.edu.ar (A.G.S.); gpr@quimica.unlp.edu.ar (G.P.R.)
4 CISAV, Cátedra de Química Orgánica, Facultad de Ciencias Agrarias y Forestales, Universidad Nacional de La Plata, La Plata B1904AAN, Argentina
5 Departamento de Química Orgánica, Grupo FQM-383, Universidad de Córdoba, 14014 Córdoba, Spain
6 Scientific Center for Molecular Design and Synthesis of Innovative Compounds for the Medical Industry, Peoples Friendship University of Russia (RUDN University), 117198 Moscow, Russia
* Correspondence: rafael.luque@uco.es; Tel.: +34-957211050

Received: 30 November 2018; Accepted: 18 January 2019; Published: 1 February 2019

Abstract: Zn/MCM-41 mesoporous materials have been prepared via classic wet impregnation, employing zinc nitrate as precursor and tested for activity and stability in the Friedel-Crafts alkylation of toluene with benzyl chloride under microwave irradiation and continuous flow. The modified materials were characterized by means of a number of analytical techniques, and surface and textural properties were thoroughly checked. Materials containing the highest Zn loading (15 wt %) provided full conversion after 5 min reaction under microwave irradiation (300 W, 120 °C). Materials were proved to be stable and reusable for several cycles with an optimum performance under continuous flow conditions.

Keywords: MCM-41; Friedel–Crafts alkylation; microwave; continuous flow; zinc

1. Introduction

The design of cost-competitive, highly active, and stable catalytic systems constitutes a significant challenge in the field of materials engineering for the 21st century [1]. Much effort has been made in recent years to investigate the use of solid acid systems, including porous aluminosilicates as alternative catalysts to homogeneous systems for acid catalyzed processes [2–4]. The use of benzyl chloride as an alkylating agent for Friedel-Crafts alkylation can provide access to substituted diphenyl derivatives—relevant intermediates in the synthesis of high added value products. Lewis acids, including $AlCl_3$, $FeCl_3$, HF, BF_3, and $ZnCl_2$, have been typically used in Friedel-Crafts alkylation [5,6]. However, recovery, separation, and disposal of homogeneous Lewis acids and their originated waste has several environmental, health, and safety issues. The utilization of solid acids, such as nanostructured materials, can provide alternative recycling and separation possibilities, minimizing pollution and waste. Alkylation reactions have been extensively catalyzed by a large variety of solid acids, such as: β-zeolites [7]; ZSM-5 modified with Ga, Zn, In, and Fe [8–11]; Fe, Ga, and Al-SBA-15

and MCM-41 supports [2,12–14]; Ga-Mg oxides and hydrotalcites [15]; and different ferrites with Cu, Ni, Co, Zn, Mg [16], among others. Although there has been some progress for more efficient Friedel-Crafts alkylation reactions, developing scalable-continuous flow and environmentally friendly procedures using stable and highly active catalysts remains a challenge.

The production of diphenylmethane from toluene alkylation requires high acidity, in addition to unhindered active sites (acid sites), to promote bulk reactions. Zeolites are acid catalysts featuring shape-selectivity able to provide specific selectivity to certain intermediates and products. However, zeolites generally possess tiny pore sizes (<1 nm), which restricts their utilization in chemistries involving bulk substrates [7]. Comparatively, ordered mesoporous silicas can exhibit promising features as alternative catalytic systems, including an appropriate use in macromolecular reactions due to their controllable mesopores (typically 2–10 nm), high specific pore volumes (up to 1.3 mL/g), and well-defined mesoporous array [17]. Due to their large internal surface generally being highly accessible, such porous materials can stabilize several active sites, such as transition metals, Brønsted and Lewis acids, metal oxide clusters, and small particles. MCM-41 can accommodate highly dispersed metal nanoparticles, in order to enhance the catalytic performance via larger number of active sites per unit area. The incorporation of aluminum, gallium, nickel, zinc, and other metals into their structure increases the acidity and thereby the catalytic function [18]. Gracia et al. [12] have reported the use of gallium and aluminum-galosilicate materials in toluene alkylation at 110 °C using benzyl chloride as an alkylating agent. Full conversion and selectivity at approximately >99% could be achieved for the monoalkylated product, with a 1/1 o-/p- ratio. Pineda et al. [2] studied the alkylation of toluene with benzyl chloride in a microwave reactor, employing mechanochemically synthesized Fe/Al-SBA-15 systems as optimum Lewis acid solid catalyst with excelling activities. Balu et al. [19] also reported the same reaction under continuous flow, employing similarly low-loaded Fe-based catalysts, able to provide good to excellent yields of alkylated products.

Herein, we report the synthesis and characterization of zinc-containing ordered mesoporous MCM-41 materials and their application in toluene alkylation using benzyl chloride under microwave irradiation. Results have also been compared to continuous flow conditions in order to benchmark the stability and the activity of the materials at industrially-closer conditions.

2. Results

2.1. Physicochemical Characterization

Textural and surface properties of synthesized materials have been presented in Table 1. In addition, zinc quantities in the catalysts, calculated by chemical analysis and expressed as Zn wt %, are also shown.

The results obtained from low-angle X-ray powder diffraction (XRD) measurements for the synthesized catalysts and the support are shown in Figure 1. MCM-41 materials exhibited all characteristics resolved diffraction lines of the hexagonal ordering in MCM-41, indexed as (1 0 0), (1 1 0), and (2 0 0) reflections [17,20]. Accordingly, Zn/MCM-41 catalysts showed a similar low-angle XRD pattern as compared to the parent material.

However, an intensity decrease accompanied by diffraction line widening could be observed at increased Zn content, pointing out a deterioration in long-range ordering. This last fact could reflect the partial structure collapse, as well as mesopore blocking upon Zn incorporation. FWHM (full width at half maximum) corresponding to the main (100) peak of the XRD patterns indeed provided hints of the widening of the peaks, which increased with the Zn loading in the support. The (100) reflection also changed slightly to higher angle, with the lattice parameter (a_0) concurrently decreasing upon long-range structural order diminishment [21].

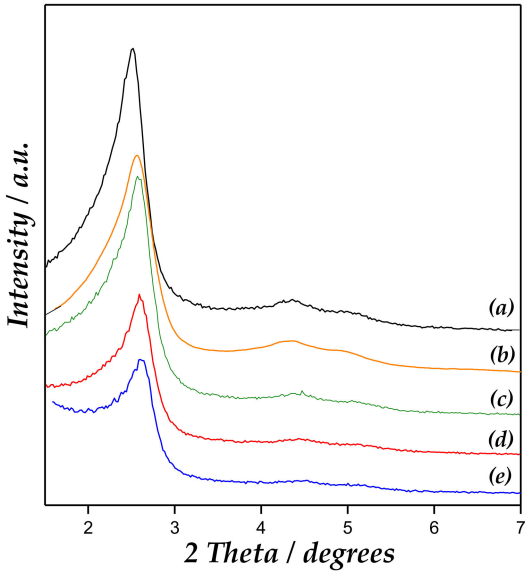

Figure 1. X-ray diffraction patterns of (a) MCM-41, (b) Zn/MCM-41(1), (c) Zn/MCM-41(2.5), (d) Zn/MCM-41(10), and (**e**) Zn/MCM-41(15) catalysts.

On the other hand, no ZnO diffraction lines could be observed in high-angle XRD patterns (Figure S2, Supplementary Materials), which suggested that Zn species were amorphous or their crystal domain size was below the detection limit for XRD (<4–6 nm). These are likely to be either finely dispersed in the framework or located at the external surface of the support [22–24].

The observed long range hexagonal ordering of Zn/MCM-41 materials and support was also corroborated by Transmission Electron Microscopy (TEM) images (Figure 2a,b), which revealed ordered hexagonal arrays of mesopores with uniform pore sizes, characteristic of MCM-41 materials [25].

The morphology of synthesized materials was examined by Scanning Electron Microscopy (SEM). Figure 2c,d show that these materials do not show any specific arrangement. Furthermore, it is possible observe aggregates with irregular shapes and an average size of 2–4 μm, supporting previous results [26].

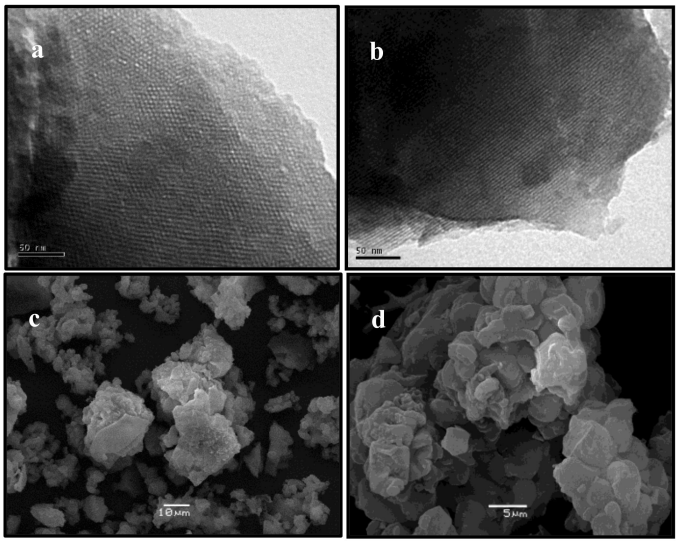

Figure 2. Transmission Electron Microscopy (TEM) and Scanning Electron Microscopy (SEM) images of (**a**–**c**) MCM-41, and (**b**–**d**) Zn/MCM-41(2.5) (taken as representative).

Figure 3 shows nitrogen adsorption–desorption isotherms at −193 °C of studied materials, and their textural properties are summarized in Table 1. All catalysts display Type IV isotherms of IUPAC

classification [27]. It is possible a decrease in the volume of gas adsorbed and in the pore volume regarding to the MCM-41 sample was observed, which could be due the formation of zinc species into the channels and onto mesoporous surface. In addition, the inflection region between p/p^0 range = 0.1–0.25 was assigned to the condensation phenomenon. The inflection is less pronounced with the increase in Zn loading, which indicates a broader pore size distribution.

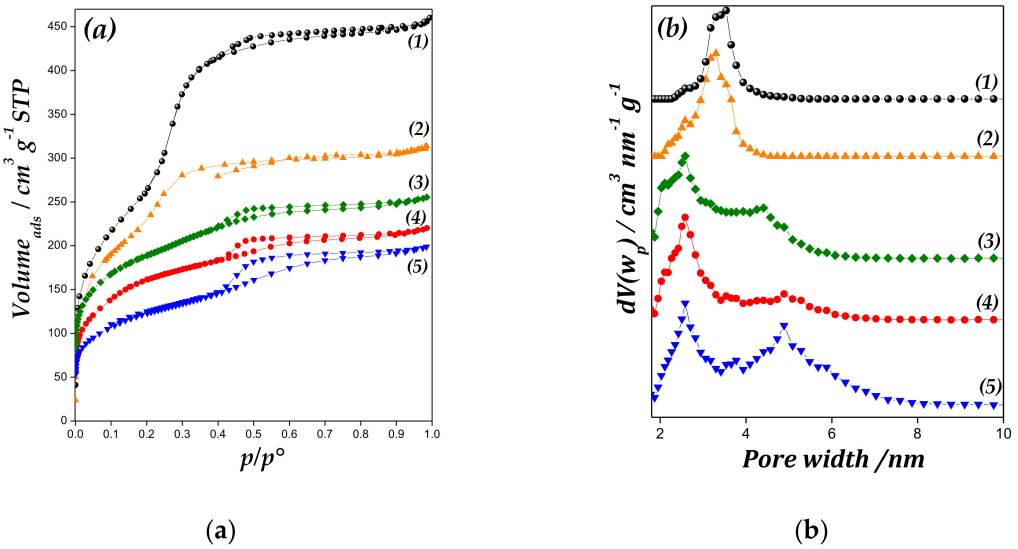

Figure 3. (**a**) Nitrogen adsorption-desorption isotherms of (1) MCM-41, (2) Zn/MCM-41(1), (3) Zn/MCM-41(2.5), (4) Zn/MCM-41(10) and (5) Zn/MCM-41(15) catalysts, and (**b**) pore size distributions (PSD) of samples.

In the pore size distributions (PSD) plot (Figure 3 inset), the average pore diameter of support and Zn/MCM-41(1) sample was approximately 3.5 nm, with narrow distribution. However, by increasing the Zn amount in the samples, the PSD broadens, displaying a bimodal PSD, although the desorption branch does not display two distinct steps. These samples present a dual mesoporous distribution, with a well-defined peak at 2.6 nm and additional wide peak around of 4–6 nm. This may be due to the partial blockage of the primary mesopores at increased zinc oxide amount, the subsequent deterioration of the structure, and the appearance of larger size pores with irregular distribution [28,29].

In addition, as is shown in Table 1, Zn/MCM-41 samples present a diminution in the textural parameters (S_{BET} and V_{TP} values). The decrease in these values with increasing Zn content implies a blockage of pore channels besides structural deterioration, due to depositing Zn species on the support.

Table 1. Textural properties of studied materials.

Sample	Zn [wt %] [a]	S_{BET} [m^2/g] [b]	V_{PM} [cm^3/g] [c]	V_{TP} [cm^3/g] [d]	Lewis Acidity [μmol Py × g^{-1}] [e]
MCM-41	-	940	0.62	0.70	-
Zn/MCM-4(1)	0.09	764	0.36	0.42	13
Zn/MCM-41(2.5)	2.65	592	0.30	0.36	14
Zn/MCM-41(10)	9.87	532	0.27	0.32	18
Zn/MCM-41(15)	14.6	370	0.22	0.27	23

[a] Estimated by Atomic Emission Spectroscopy (ICP). [b] Estimated by Brunauer-Emmett-Teller (BET) method. [c] Primary mesopore volume. [d] Pore volume. [e] Estimated by Fourier transform infrared (FTIR)-pyridine studies.

UV-Vis spectra of Zn/MCM-41 samples and bulk ZnO are presented in Figure 4. A strong band at 280–380 nm for Zn/MCM-41 catalysts is associated with the presence of ZnO particles. It is well-known that ZnO powders present an intense absorption peak between 370 and 330 nm [30,31]. However, in semiconductors, the blue shift of absorption band edge towards lower wavelength indicates a quantum size effect. Accordingly, this absorption band increases in intensity and displacement towards higher wavenumber with metallic content growth, accounting for larger ZnO species.

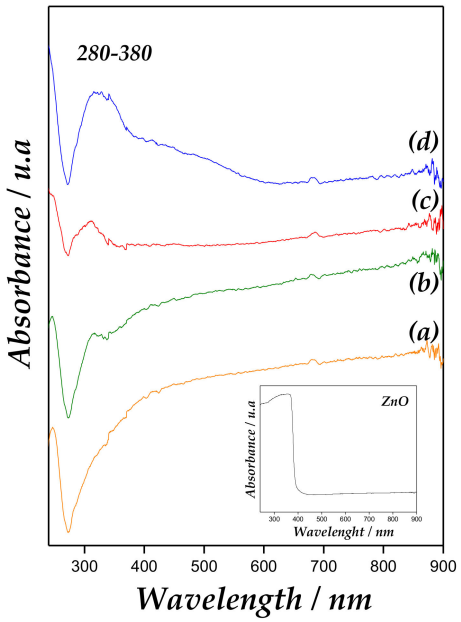

Figure 4. Diffuse Reflectance Ultraviolet-Visible Spectroscopy (DRUV–Vis) spectra of (a) Zn/MCM-41(1), (b) Zn/MCM-41(2.5), (c) Zn/MCM-41(10), and (d) Zn/MCM-41(15) catalysts.

Additionally, X-ray photoelectron spectroscopy (XPS) is a useful technique to confirm presence of ZnO. XPS of Zn 2p (Figure 5) revealed the binding energies (BE) at approximately 1022.8 eV and 1045.7 eV, corresponding to Zn $2p^{3/2}$ and Zn $2p^{1/2}$, respectively, giving a spin-orbit splitting (SOS) of ~22.9 eV. This corroborates that Zn is in the Zn^{+2} chemical state [32]. In addition, spin-orbit splitting is well known to be 22.2 eV in pure ZnO.

These findings pointed out that ZnO would not be predominantly "bulk" ZnO, but probably as ZnO species highly dispersed and interacting with the support surface, according to Carlson [33].

The Si 2p signal in was approximately 104.4 eV, in good agreement with SiO_2-type material. Likewise, oxygen contribution in Zn/MCM-41 samples showed a symmetric peak centered at 533.3 eV, mainly due to the O^{2-} in SiO_2 [34]. Other oxygen peaks attributable to ZnO oxide and to weakly adsorbed OH^- were not detected, probably for the oxygen signal intensity of the siliceous material [35].

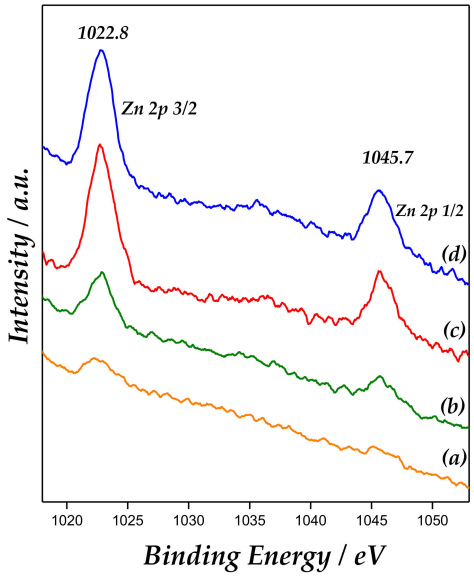

Figure 5. X-ray photoelectron spectroscopy (XPS) spectra of Zn $2p^{3/2}$ and Zn $2p1^{/2}$ for the catalysts: (a) Zn/MCM-41(1), (b) Zn/MCM-41(2.5), (c) Zn/MCM-41(10), and (d) Zn/MCM-41(15).

The binding energies, Zn/Si (surface), and Zn/Si (bulk) values, as well as Zn surface atomic and bulk concentrations for all samples, are summarized in Table 2. The metal/Si (surface) ratio corresponds to the dispersion of metal on the mesoporous support. In addition, the Zn/Si (surface) ratios are comparably reduced regarding Zn/Si (bulk) ratios, due to the fact Zn species would be incorporated mostly within the mesopores as clusters or very small nanoparticles. However, the zinc species would not be homogeneously dispersed on the siliceous mesoporous framework.

Table 2. Binding energies values (eV) for Zn 2p spectra and surface Zn/Si compositions of Zn/MCM-41(x) samples and reference ZnO.

Sample	Zn $2p^{3/2}$ [eV]	Zn $2p^{1/2}$ [eV]	Zn/Si (Surface) [a]	Zn/Si (Bulk) [b]	Zn [at. %] [a]	Bulk Zn [wt %] [b]
Zn/MCM-41(1)	1022.9	1045.7	0.003	<0.001	0.10	0.09
Zn/MCM-41(2.5)	1022.1	1045.5	0.004	0.025	0.20	2.65
Zn/MCM-41(5)	1022.4	1045.7	0.007	0.041	0.20	4.29
Zn/MCM-41(10)	1022.7	1045.6	0.013	0.100	0.40	9.87
Zn/MCM-41(15)	1023.1	1045.8	0.015	0.157	0.50	14.6
ZnO	1020.0	1045.0	-	-	-	-

[a] Calculated by X-ray photoelectron spectroscopy (XPS), [b] calculated by Atomic Emission Spectroscopy (ICP).

The spectroscopic study of the chemisorption of pyridine (Py) is usually a useful method that allows an evaluation of the amount and strength of the acid centers on a catalyst surface [36]. To investigate the acidic strengths of Lewis (L) and Brønsted (B) sites, the pyridine thermodesorption was carried out. IR spectra at different temperatures are displayed in Figure 6.

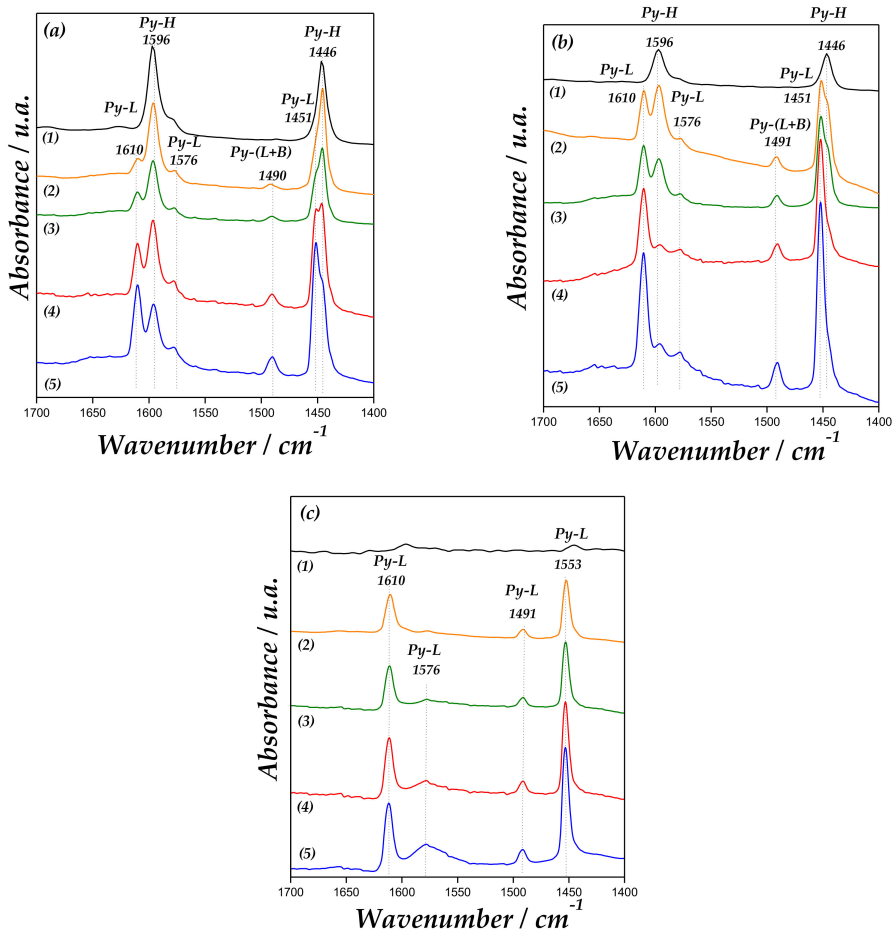

Figure 6. Fourier transform infrared (FT-IR) spectra of (1) MCM-41, (2) Zn/MCM-41(1), (3) Zn/MCM-41(2.5), (4) Zn/MCM-41(10), and (5) Zn/MCM-41(15), containing adsorbed pyridine and subsequent desorption at 50 °C (a), 100 °C (b) and 200 °C (c).

SiOH groups interact with pyridine through hydrogen bonding. All samples presented bands at 1446 and 1596 cm^{-1} due to hydrogen-bonded pyridine (H-Py) [37,38]. These band are not present after the evacuation at 200 °C due to the weakness of the site [33,34]. In addition, the Zn/MCM-41 samples also show the bands of H-Py (1446 and 1596 cm^{-1}), Lewis-bonded pyridine (L-Py: 1451, 1576 and 1610 cm^{-1}), and a band at 1491 cm^{-1} due to interaction of pyridine over (L + B) acid sites [39]. As observed in Figure 6, the intensity of bands at 1610 and 1451 cm^{-1}, corresponding to Py interaction with Lewis acid sites, increases with the Zn loading on the support. The band at 1576 cm^{-1} corresponds to the vibration of adsorbed pyridine to weak surface Lewis acid sites. Moreover, bands corresponding to Brønsted acid sites at 1540 and 1636 cm^{-1} were not detected [40]. Therefore, the band at 1491 cm^{-1} is only associated with Lewis acid sites, which increase with the amount of zinc in the material. Accordingly, it is possible to observe that these bands assigned to Lewis sites are maintained until 200 °C, indicating their acidic strength. Thus, these sites can mainly be associated with a strong electron-donor-acceptor adduct of the probe molecule with Lewis-type sites, attributed to isolated zinc species coordinated to framework oxygen atoms (Zn unoccupied molecular orbital) interacting with pyridine.

Figure 7 displays the Fourier transform infrared (FT-IR) region of hydroxyl of the catalyst after Py adsorption followed by desorption at 200 °C. MCM-41 spectrum exhibit a band at approximately 3740 cm^{-1} assigned to isolated terminal O-H group [41,42]. In addition, a decrease of intensity and broadening of this band is evidenced for Zn/MCM-41 samples. The widening of this band is assigned to Zn-OH surface species, whereby an interaction would occur between the vicinal OH groups, such as Si-OH and Zn-OH groups. However, a decrease of this band could be due to a partial blocking of Si-OH groups from the coordination of the Si-OH groups with Zn ions, leading to the bonds of Si-O-Zn. This last has been already reported by us [21,37].

The molar extinction coefficient of the Lewis acid site-adsorbed pyridine band was employed to estimate concentration of the acid sites of the samples [43]. The acidity concentrations (μmol pyridine × g^{-1}) are given in Table 1. Thus, the acid sites increase with the Zn amount in the MCM-41 support.

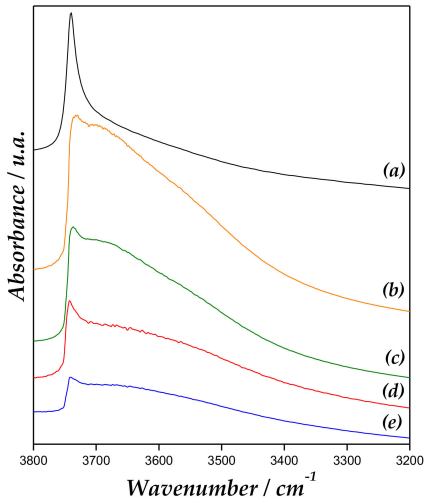

Figure 7. FT-IR region of OH after pyridine adsorption and desorption of (a) MCM-41, (b) Zn/MCM-41(1), (c) Zn/MCM-41(2.5), (d) Zn/MCM-41(10), and (e) Zn/MCM-41(15) at 200 °C.

2.2. Catalytic Activity

2.2.1. Alkylation Reaction Under Microwave Irradiation

Initially, the alkylation reaction of toluene (Tol) with benzyl chloride (BC) was conducted under microwave irradiation (120 °C, 300 W), with the goal of finding optimal conditions and the best catalyst (Scheme 1).

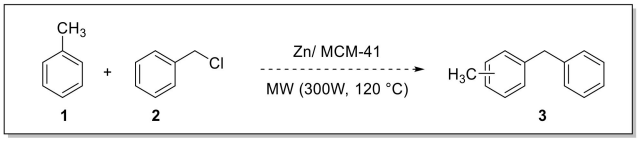

Scheme 1. Alkylation of toluene (Tol) employed benzyl chloride (BC) under microwave irradiation.

Data are summarized in Table 3. This alkylation was first carried out using MCM-41 (25 mg), Tol (2.0 mL), and BC (0.1 mL). After 5 and 10 min, the products formation was not detected (Table 3, Entry 1). Similarly, if the reaction is carried out without catalyst, the formation of products is not observed (Table 3, Entry 2).

The initial use of Zn/MCM-41(1) indicates that when 12.5 mg catalyst, 1.0 mL toluene, and 0.1 mL benzyl chloride are used, a better conversion is observed after 10 min of reaction (Table 3, Entry 5). Interestingly, a higher conversion at approximately 80% could be obtained when the zinc loading on MCM-41 was increased for catalysts Zn/MCM-41(2.5) and Zn/MCM-41(10) (Table 3, Entries 6 and 7). Observed products were primarily the ortho and para isomers, and a small amount of the meta isomer, as expected for an electrophilic aromatic substitution of toluene. All catalysts exhibited selectivity higher than 90% to the desired mono alkylated products, with a near 1/1 (ortho/para) ratio. In addition, the molecular sizes were calculated by HyperChem v5.0 (Hypercube, Inc., Gainesville, FL, USA) (see Supplementary Materials) in order to confirm there were no diffusion-limiting problems.

Table 3. Activities and selectivity of Zn/MCM-41 in the alkylation of toluene with benzyl chloride under microwave irradiation [(a)].

#	Toluene [mL]	BzCl [mL]	Catalysts [mg]	Time [min]	X_T [%]	S_{ortho} [%]	S_{meta} [%]	S_{para} [%]
1	2.0	0.1	MCM-41 (25 mg)	5	-	-	-	-
				10	-	-	-	-
2	2.0	0.1	-	5	-	-	-	-
				10	-	-	-	-
3	2.0	0.1	Zn/MCM-41(1) (12.5 mg)	5	25	40	6	54
				10	47	39	6	55
4	2.0	0.1	Zn/MCM-41(1) (25 mg)	5	14	39	7	54
				10	31	35	8	57
				15	52	39	6	55
5	1.0	0.1	Zn/MCM-41(1) (12.5 mg)	5	56	40	6	54
				10	63	35	8	57
6	1.0	0.1	Zn/MCM-41(2.5) (12.5 mg)	5	53	39	6	55
				10	77	38	6	56
				15	81	39	5	56
7	1.0	0.1	Zn/MCM-41(10) (12.5 mg)	5	45	41	7	52
				10	69	40	7	53
				15	80	40	6	54
8	1.0	0.1	Zn/MCM-41(15) (12.5 mg)	5	>99	41	6	53
				10	>99	40	6	54
				15	>99	41	6	53
9	1.0	0.1	Zn/MCM-41(15) (6.25 mg)	5	46	40	6	54
				10	56	39	6	55
				15	58	39	6	55

[(a)] Reaction conditions: toluene, benzyl chloride, catalyst, MW (120 °C, 300W). (XT, %) Total conversion; (Sortho, %) 2-methyl diphenylmethane; (Smeta, %) 3-methyl diphenylmethane; (Spara, %) 4 methyl diphenylmethane.

On the other hand, the maximum conversion in the process was obtained for Zn/MCM-41(15), leading to quantitative product yields in only 5 min of reaction (Table 3, Entry 8). In search of the ideal amount of catalyst, the reaction was tested using 6.25 mg of Zn/MCM-41(15), but unfortunately there was a decrease in product conversion (Table 3, Entry 9).

For a long time, Lewis acids have been reported to promote this type of reaction, being the determining factor [5]. As has already been observed, the increase of zinc loading is responsible for the acidity increase in the catalyst. Zn/MCM-41(15) catalyst, exhibiting the highest conversion, has the highest zinc loading and highest acidity. However, the acidity of the materials is not the only important factor in the catalytic activity of the systems, since all materials exhibited relatively similar surface

acid properties, particularly at moderate to high temperatures (Py titration data, Figure 6). The highest activity measured for Zn/MCM-41(15) could be associated not only with a slightly increased acidity but also with its textural properties. This material exhibited a marked dual mesoporous distribution, which was related to the structural deterioration and appearance of larger size pores with irregular distribution in the defective structure. This fact would probably contribute to enhancing the interaction between the reactant and catalyst, besides the accessibility to active sites, favoring the higher catalytic activity observed for this sample. The mesoporous surface area effect, on the alkylation reaction, has been reported by Milina et al. [44].

2.2.2. Catalyst Reuse Studies Under Microwave Irradiation

The reusability of Zn/MCM-41(15) was subsequently investigated under microwave irradiation conditions with results included in Figure 8. The odd reuse numbers (1st, 3rd, and 5th) correspond to the reaction with regenerated material (calcinated at 400 °C in air, 2 h) and the pair reuses (2nd and 4th) are those without reactivations treatment. This test was carried out under the best conditions found (1 mL toluene, 0.1 mL benzyl chloride and 12.5 mg catalyst at 120 °C, 5 min reaction), for which reactions were stopped after a few minutes halfway through the reaction, and then the mixture was filtered off in order to separate the catalysts, and this was washed with toluene and kept in an oven at 100 °C for 1 h prior to its use in the next alkylation reaction (1st reuse), for which quantitative conversion was found. The second reuse of the catalyst, under identical reaction conditions and without reactivation, provided a much reduced conversion (56%) with similar selectivity (2nd reuse). The decrease of the total conversion could be attributed to the presence of organic species adsorbed on the catalytic material surface. For the 3rd reuse, the catalyst was calcined in air at 400 °C for 2 h, again providing quantitative conversion after 5 min of reaction. The 4th reuse, without reactivation, provided a reduced conversion with similar selectivity as the 2nd reuse. Thus, the regenerated materials could again provide quantitative conversion after 5 min of reaction (3rd and 5th reuses). Therefore, the catalyst was found to be stable, and its deactivation was not due to Zn leaching in the first few reuses or regenerations. Nevertheless, these results clearly demonstrated a high stability of the catalytic material under the investigated reaction conditions, preserving almost unchanged initial activity after several cycles.

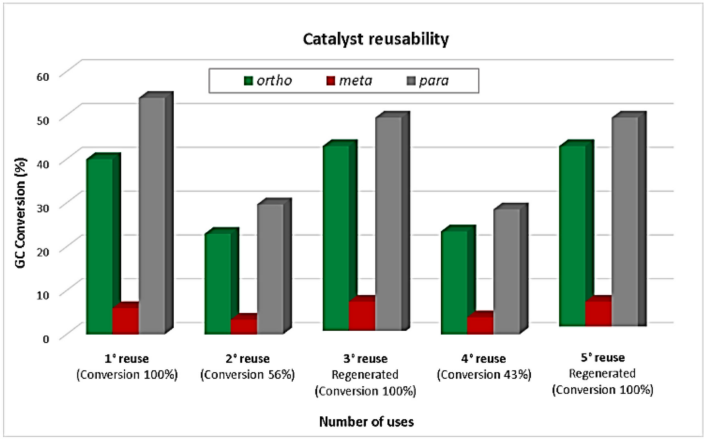

Figure 8. Reusability experiments of Zn/MCM-41(15) in the alkylation of toluene with benzyl chloride. Reaction conditions: 1 mL toluene, 0.1 mL benzyl chloride, 12.5 mg Zn/MCM-41(15), 5 min, MWs, 120 °C, 300 W.

2.2.3. Continuous Flow Alkylation Reaction: Activity and Stability

Additionally, the reaction was performed under continuous flow conditions in order to test the activity, but most importantly the stability of the synthesized materials, focusing on optimum Zn/MCM-41(15). Reaction conditions (120 °C, 0.4 mL/min, 110 mg of catalysts) were translated from

microwave to continuous flow, taking advantage of the moderate temperatures and pressures in the microwave reactor that could be mimicked in a continuous flow system. [45]. Results are summarized in Table 4.

Initially, Zn/MCM-41(15) catalyst exhibited a >99% conversion to alkylation products in the first 15 min of reaction (equivalent to a residence time of 0.6 min, see Table 4). After 165 min of reaction in continuous flow at 100 °C, we can observe a conversion decrease from >99 to 80%, while the selectivity remained practically constant throughout the process (Table 4). Most importantly, a long reaction run (20 h, Table 4 last entry) also indicated that the catalyst was rather stable with time on stream under continuous flow (72% conversion) after the observed initial activity drop due to (1) a minor leaching (<20 ppm) observed, probably of weakly coordinated Zn species in the materials and the leaching effect of generated HCl, and (2) the presence of strongly adsorbed aromatics that can be eliminated upon regeneration (i.e., calcination). Particularly, the stability of the materials under flow conditions was remarkable and further supported the reusability results under microwave irradiation, probably improved due to the low residence time of byproduct HCl in the catalyst under flow conditions that decreased Zn leaching.

Table 4. Activities and selectivity of Zn/MCM-41 in the alkylation of toluene with benzyl chloride in flow chemistry [(a)].

Catalyst	Time [min] [(b)]	X_T [%]	S_2 [%]	S_3 [%]	S_4 [%]
Zn/MCM-41(15)	15 (0.6)	>99	40	6	54
	45 (2.0)	88	41	6	53
	75 (3.3)	89	42	6	52
	105 (4.6)	85	41	7	52
	135 (6.0)	77	43	6	51
	165 (7.3)	80	44	6	50
	1200 (53.3)	72	42	6	52

[(a)] Experimental conditions: 94 mmol Tol, 10 mmol BC, 110 mg catalyst, 120 °C (0.4 mL/min). [(b)] Residence time (minutes) from the feed in the catalyst in brackets. (XT, %) Total conversion; (Sortho, %) 2-methyl diphenylmethane; (Smeta, %) 3-methyl diphenylmethane; (Spara, %) 4 methyl diphenylmethane.

3. Materials and Methods

3.1. Catalyst Preparation

The pure siliceous mesoporous material (MCM-41) was prepared following the pathway reported by Elías et al. [17]. Zn/MCM-41 catalysts were prepared by the wet impregnation method using zinc nitrate salt as precursor. For additional experimental details, see Supplementary Materials.

3.2. Characterization

Zn content was quantified using inductively coupled plasma-atomic emission spectroscopy (ICP-AES) using a spectrophotometer VISTA-MPX CCD Simultaneous ICP-OES-VARIAN (Varian, Inc., Palo Alto, CA, USA). The samples were previously digested with HF and HNO3.

Sample characterization was conducted using X-ray powder diffraction (XRD), Cu Kα radiation (λ = 1.5418 Å) and measured with a PANalytical X'Pert PRO diffractometer (Philips, Almelo, The Netherlands) in the range of 2θ from 1.5 to 7° and from 10 to 80°.

N_2 adsorption-desorption isotherms were recorded at −196 °C (N_2 with 99.999% purity) in a Micromeritics ASAP 2000 instrument (Norcross, GA, USA), in order to provide information on textural properties. Scanning Electron Microscopy (SEM) was also employed to visualize the catalyst morphology, for which a JEOL JSM-6380 LV (Tokyo, Japan) (20kV acceleration voltage) and gold sputtering was utilized to coat the samples in order to maximize their beam stability.

Fourier transform infrared (FT-IR) data was performed on a Nicolet iS10 FTIR spectrometer (Thermo Scientific, Waltham, MA, USA). For full experimental details, see Supplementary Materials.

3.3. Catalytic Experiments

Toluene alkylation with benzyl chloride and the reusability experiments were carried out using a CEM-DISCOVER microwave synthesizer (Matthews, NC, USA), in an open vessel under continuous stirring.

Continuous flow experiments were conducted in a high-temperature high-pressure Phoenix Flow Reactor (ThalesNanoTM, Budapest, Hungary) connected to a HPLC pump. For experimental details, see Supplementary Materials.

4. Conclusions

Zn-containing MCM-41 catalysts was prepared with varying zinc contents and evaluated in the alkylation reaction of toluene using microwaves and flow chemistry, as well as benzyl chloride as alkylating agent. Zn/MCM-41 featured typical high surface areas and hexagonal arrangements. However, higher Zn loading originated a partial collapse in structure. The acidity of the catalysts increased with the highest Zn loading, which was reflected in the increase of the catalytic activity. The large mesopores of the catalysts did not pose any constraints on the reaction intermediates and products, as opposed to microporous materials.

Zn/MCM-41(15) exhibited the best activity and selectivity to the desired products (o- and p-methyl diphenylmethane) in the selected reaction. In addition, the mesoporous catalysts were highly stable and reusable after several reuses or regeneration cycles, both employing microwave-assisted irradiation as well as, most importantly, in a flow reactor. Based on these findings, Zn-modified MCM-41 type molecular sieves are highly suitable solid acid candidates for Friedel-Crafts alkylation.

Supplementary Materials: The following are available online at http://www.mdpi.com/2073-4344/9/2/136/s1, Table S1: Size of the reagent and product molecules calculated by HyperChem 5.0, Figure S1. FT-IR spectra of catalysts and Experimental details.

Author Contributions: All authors have participated in the discussion and writing of this work. P.M.C. synthesis and characterization of catalytic materials; B.S.G. and A.G.S. catalytic tests.

Funding: This research was funded by CONICET and UTN-FRC. A.G.S. and G.P.R. thank CONICET (PIP 0084), MINCYT (PICT 0409) and ERANET LAC-1 for the financial support. B.S.G. gratefully acknowledges support from CAPES (PDSE - 88881.133371/2016-01). The publication was prepared with support from RUDN University Program 5-100.

Conflicts of Interest: The authors declare no conflict of interest.

References

1. Wang, Y.; Arandiyan, H.; Scott, J.; Bagheri, A.; Dai, H.; Amala, R. Recent advances in ordered meso/macroporous metal oxides for heterogeneous catalysis: A review. *J. Mater. Chem. A* **2017**, *5*, 8825–8846. [CrossRef]
2. Pineda, A.; Balu, A.M.; Campelo, J.M.; Luque, R.; Romero, A.A.; Serrano-Ruiz, J.C. High alkylation activities of ball-milled synthesized low-load supported iron oxide nanoparticles on mesoporous aluminosilicates. *Catal. Today* **2012**, *18*, 765–769. [CrossRef]
3. Jin, H.; Bismillah Ansari, M.; Jeong, E.Y.; Park, S.E. Effect of mesoporosity on selective benzylation of aromatics with benzyl alcohol over mesoporous ZSM-5. *J. Catal.* **2012**, *291*, 55–62. [CrossRef]
4. Salavati-Niasari, M.; Hasanalian, J.; Najafian, H. Alumina-supported $FeCl_3$, $MnCl_2$, $CoCl_2$, $NiCl_2$, $CuCl_2$, and $ZnCl_2$ as catalysts for the benzylation of benzene by benzyl chloride. *J. Mol. Catal. A: Chem.* **2004**, *209*, 209–214. [CrossRef]
5. Olah, G.A. *Friedel–Crafts Chemistry*; Wiley: New York, NY, USA, 1973.
6. Olah, G.A.; Prakash, G.K.S.J.; Sommer, J. *Superacids*; Wiley: New York, NY, USA, 1985.
7. Narender, N.; Krishna Mohan, K.V.V.; Kulkarni, S.J.; Ajit Kumar Reddy, I. Liquid phase benzylation of benzene and toluene with benzyl alcohol over modified zeolites. *Catal. Commun.* **2006**, *7*, 583–588. [CrossRef]
8. Choudhary, V.R.; Jana, S.K.; Kiran, B.P. Alkylation of benzene by benzyl chloride over H-ZSM-5 zeolite with its framework Al completely or partially substituted by Fe or Ga. *Catal. Lett.* **1999**, *59*, 217–219. [CrossRef]

9. Choudhary, V.R.; Jana, S.K. Benzylation of benzene by benzyl chloride over Fe-, Zn-, Ga- and In-modified ZSM-5 type zeolite catalysts. *Appl. Catal. A* **2002**, *22*, 451–462. [CrossRef]
10. Choudhary, V.R.; Jana, S.K. Benzylation of benzene and substituted benzenes by benzyl chloride over $InCl_3$, $GaCl_3$, $FeCl_3$ and $ZnCl_2$ supported on clays and Si-MCM-41. *J. Mol. Catal. A: Chem.* **2002**, *180*, 267–276. [CrossRef]
11. Choudhary, V.R.; Mulla, S.A.R.; Banerjee, S. Aromatization of n-heptane over H-AlMFI, Ga/H-AlMFI, H-GaMFI and H-GaAlMFI zeolite catalysts: Influence of zeolitic acidity and non-framework gallium. *Mesoporous Mater.* **2003**, *57*, 317–322. [CrossRef]
12. Gracia, M.J.; Losada, E.; Luque, R.; Campelo, J.M.; Luna, D.; Marinas, J.M.; Romero, A.A. Activity of Gallium and Aluminum SBA-15 materials in the Friedel-Crafts alkylation of toluene with benzyl chloride and benzyl alcohol. *Appl. Catal. A* **2008**, *349*, 148–155. [CrossRef]
13. Chiu, J.J.; Pine, D.J.; Bishop, S.T.; Chmelka, B.F. Friedel-Crafts alkylation properties of aluminosilica SBA-15 meso/macroporous monoliths and mesoporous powders. *J. Catal.* **2004**, *221*, 400–412. [CrossRef]
14. El Berrichi, Z.; Cherif, L.; Orsen, O.; Fraissard, J.; Tessonnier, J.P.; Vanhaecke, E.; Louis, B.; Ledoux, M.J.; Pham-Huu, C. Ga doped SBA-15 as an active and stable catalyst for Friedel–Crafts liquid-phase acylation. *Appl. Catal. A* **2006**, *298*, 194–202. [CrossRef]
15. Choudhary, V.R.; Jana, S.K.; Narkhede, V.S. Benzylation and benzoylation of substituted benzenes over solid catalysts containing Ga- and Mg-oxides and/or chlorides derived from Ga–Mg-hydrotalcite by its HCl pre-treatment or calcination. *Appl. Catal. A* **2002**, *235*, 207–215. [CrossRef]
16. Shinde, M.M.; Sawant, M.R. Liquid Phase Friedel-Crafts Alkylation over Mixed Metal Oxide Catalyst. *J. Chin. Chem. Soc.* **2003**, *50*, 1221–1226. [CrossRef]
17. Elías, V.; Crivello, M.; Herrero, E.; Casuscelli, S.; Eimer, G. Some considerations to optimize the synthesis procedure and the structural quality of mesostructured silicas. *J. Non-Cryst. Solids* **2009**, *355*, 1269–1273. [CrossRef]
18. Vaschetto, E.G.; Pecchi, G.A.; Casuscelli, S.G.; Eimer, G.A. Nature of the active sites in Al-MCM-41 nano-structured catalysts for the selective rearrangement of cyclohexanone oxime toward e-caprolactam. *Micropor. Mesopor. Mater.* **2014**, *200*, 110–116. [CrossRef]
19. Balu, A.M.; Pineda, A.; Obermayer, D.; Romero, A.A.; Kappe, C.O.; Luque, R. Versatile low-loaded mechanochemically synthesized supported iron oxide nanoparticles for continuous flow alkylations. *RSC Adv.* **2013**, *3*, 16292–16295. [CrossRef]
20. Corma, A. From microporous to mesoporous molecular sieve materials and their use in catalysis. *Chem. Rev.* **1997**, *97*, 2373–2419. [CrossRef]
21. Carraro, P.M.; Elías, V.R.; García Blanco, A.A.; Sapag, K.; Moreno, S.; Oliva, M.I.; Eimer, G.A. Synthesis and multi-technique characterization of nickel loaded MCM-41 as potential hydrogen-storage materials. *Micropor. Mesopor. Mater.* **2014**, *191*, 103–111. [CrossRef]
22. Lihitkar, P.B.; Violet, S.; Shirolkar, M.; Singh, J.; Srivastava, O.N.; Naik, R.H.; Kulkarni, S.K. Confinement of zinc oxide nanoparticles in ordered mesoporous silica MCM-41. *Mater. Chem. Phys.* **2012**, *133*, 850–856. [CrossRef]
23. Jiang, Q.; Wu, Z.Y.; Wang, Y.M.; Cao, Y.; Zhou, C.F.; Zhu, J.H. Fabrication of photoluminescent ZnO/SBA-15 through directly dispersing zinc nitrate into the as-prepared mesoporous silica occluded with template. *Mater. Chem.* **2006**, *16*, 1536–1542. [CrossRef]
24. Chen, H.G.; Shi, J.L.; Chen, H.R.; Yan, J.N.; Li, Y.S.; Hua, Z.L.; Yang, Y.; Yan, D.S. The preparation and photoluminescence properties of ZnO-MCM-41. *Opt. Mater.* **2004**, *25*, 79–84. [CrossRef]
25. Bengoa, J.; Cagnoli, M.; Gallegos, N.; Alvarez, A.; Mogni, L.; Moreno, M.; Marchetti, S. Iron oxide nanoparticles inside the MCM-41 channels: study of the structural stability of the support. *Micropor. Mesopor. Mater.* **2005**, *84*, 153–160. [CrossRef]
26. Savidha, R.; Pandurangan, A. Vapour phase isopropylation of phenol over zinc- and iron-containing Al-MCM-41 molecular sieves. *Appl. Catal. A* **2004**, *262*, 1–11. [CrossRef]
27. Everett, D.H. Manual of symbols and terminology for physicochemical quantities and units Appendix II. In *Definitions, Terminology and Symbols in Colloid and Surface Chemistry*; Part I; IUPAC Council: Washington DC, USA, 1971.
28. Do, Y.; Kim, J.; Park, J.; Park, S.; Hong, S.; Suh, C.; Lee, G. Photocatalytic decomposition of 4-nitrophenol on Ti-containing MCM-41. *Catal. Today* **2005**, *101*, 299–305. [CrossRef]

29. Rouquerol, F.; Rouquerol, J.; Sing, K. Principles, methodology and application. In *Adsorption by Powders and Porous Solids*; Academic Press: Cambridge, MA, USA, 1999.
30. Collard, X.; Louette, P.; Fiorilli, S.L.; Aprile, C. High surface area zincosilicates as efficient catalysts for the synthesis of ethyl lactate: An in-depth structural investigation. *Phys. Chem. Chem. Phys.* **2015**, *17*, 26756–26765. [CrossRef] [PubMed]
31. Mihai, G.D.; Meynen, V.; Mertens, M.; Bilba, N.; Cool, P.; Vansant, E.F. ZnO nanoparticles supported on mesoporous MCM-41 and SBA-15: a comparative physicochemical and photocatalytic study. *J. Mater. Sci.* **2010**, *45*, 5786–5794. [CrossRef]
32. Dupin, J.-C.; Gonbeau, D.; Vinatier, P.; Levasseur, A. Systematic XPS studies of metal oxides, hydroxides and peroxides. *Phys. Chem. Chem. Phys.* **2000**, *2*, 1319–1324. [CrossRef]
33. Carlson, T.A. *Photoelectron and Auger Spectroscopy*; Springer US: New York, NY, USA, 1975.
34. Shen, S.; Chen, J.; Koodali, R.T.; Hu, Y.; Xiao, Q.; Zhou, J.; Wang, X.; Guo, L. Activation of MCM-41 mesoporous silica by transition-metal incorporation for photocatalytic hydrogen production. *Appl. Catal. B* **2014**, *150–151*, 138–146. [CrossRef]
35. De Stefanis, A.; Kaciulis, S.; Pandolfi, L. Preparation and characterization of Fe-MCM-41 catalysts employed in the degradation of plastic materials. *Micropor. Mesopor. Mater.* **2007**, *99*, 140–148. [CrossRef]
36. Parry, E.P. An Infrared Study of Pyridine Adsorbed on Acidic Solids. *J. Catal.* **1963**, *2*, 371–379. [CrossRef]
37. Eimer, G.A.; Casuscelli, S.G.; Chanquia, C.M.; Elías, V.; Crivello, M.E.; Herrero, E.R. The influence of Ti-loading on the acid behavior and on the catalytic efficiency of mesoporous Ti-MCM-41 molecular sieves. *Catal. Today* **2008**, *133–135*, 639–646. [CrossRef]
38. Chakraborty, B.; Viswanathan, B. Surface acidity of MCM-41 by in situ IR studies of pyridine adsorption. *Catal. Today* **1999**, *49*, 253. [CrossRef]
39. Selvaraj, M.; Lee, T.G. t-Butylation of toluene with t-butyl alcohol over mesoporous Zn-Al-MCM-41 molecular sieves. *Micropor. Mesopor. Mater.* **2005**, *85*, 59–74. [CrossRef]
40. Chanquía, C.; Andrini, L.; Fernandez, J.; Crivello, M.; Requejo, F.; Herrero, E.; Eimer, G. Speciation of Copper in Spherical Mesoporous Silicates: From the Microscale to Angstrom. *J. Phys. Chem. C* **2010**, *114*, 12221–12229. [CrossRef]
41. Gao, F.; Zhang, Y.; Wan, H.; Kong, Y.; Wu, X.; Dong, L.; Li, B.; Chen, Y. The states of vanadium species in V-SBA-15 synthesized under different pH values. *Micropor. Mesopor. Mater.* **2008**, *110*, 508. [CrossRef]
42. Segura, Y.; Cool, P.; Kustroeski, P.P.; Chmielarz, L.; Dziembaj, R.; Vansant, E.F. Characterization of Vanadium and Titanium Oxide Supported SBA-15. *J. Phys. Chem. B* **2005**, *109*, 12071. [CrossRef]
43. Emeis, C.A. Determination of Integrated Molar Extinction Coefficients for Infrared Absorption Bands of Pyridine Adsorbed on Solid Acid Catalysts. *J. Catal.* **1993**, *141*, 347–354. [CrossRef]
44. Milina, M.; Mitchell, S.; Trinidad, Z.D.; Verboekend, D.; Pérez-Ramírez, J. Decoupling porosity and compositional effects on desilicated ZSM-5 zeolites for optimal alkylation performance. *Catal. Sci. Tlechno.* **2012**, *2*, 759–766. [CrossRef]
45. Glasnov, T.N.; Kappe, C.O. The microwave-to-flow paradigm: translating high-temperature batch microwave chemistry to scalable continuous-flow processes. *Chem. Eur. J.* **2011**, *17*, 11956–11968. [CrossRef] [PubMed]